SCIENTIFIC Publishing Limited

New Energy Exploitation and Application

https://ojs.ukscip.com/index.php/neea

Article

Experimental Validation and Performance Analysis of Flux Switching Permanent Magnet Machines Using the Virtual Current Method for EV/HEV Applications

Ehsan Shirzad

Department of Electrical and Electronics Engineering, Turan Institute of Higher Education, Damghan 3671911311, Iran; Ehsan_shirzad_72@yahoo.com

Received: 12 November 2025; **Revised:** 24 December 2025; **Accepted:** 29 December2025; **Published:** 8 January 2026

Abstract: This paper experimentally validates the Virtual Current Method (VCM) for predicting the air-gap magnetic field and performance of a 12/10 Flux Switching Permanent Magnet (FSPM) machine. Unlike prior VCM studies, which are mainly limited to analytical derivation or numerical verification, this work provides a full experimental assessment using a fabricated FSPM prototype. The prototype was designed based on the proposed analytical model, and a dedicated test bench was developed to measure back-electromotive force (EMF), electromagnetic torque, and air-gap flux density under various load conditions. Experimental measurements are systematically compared with both analytical predictions and 2D finite element method (FEM) simulations. Results show that the VCM-based model predicts the air-gap flux density with a maximum deviation of 3.6% from experiments and 2.8% from FEM. The prototype delivers an average torque of 5.4 N · m at 5 A root mean square (RMS) phase current, achieving a power factor of 0.89 and efficiency above 93%. These findings confirm that the proposed VCM formulation provides a reliable, low-computational-cost, and experimentally validated tool suitable for preliminary design and performance optimization of FSPM machines. The study highlights the practical applicability of VCM, bridging the gap between analytical models and experimental performance evaluation in advanced electric machine design.

Keywords: Flux Switching Permanent Magnet (FSPM) Machine; Virtual Current Method (VCM); Experimental Validation; Back-EMF; Torque Measurement; Finite Element Method (FEM)

1. Introduction

The increasing demand for high-efficiency and high-power-density electric drives has accelerated research on advanced motor topologies suitable for hybrid and electric vehicle (HEV/EV) propulsion systems [1–3]. Among the emerging candidates, flux-switching permanent magnet (FSPM) machines showed in **Figure 1** have received significant attention because of their unique electromagnetic structure, in which both the permanent magnets (PMs) and armature windings are located on the stator, while the rotor remains a simple salient structure without windings or magnets [4,5]. This configuration offers inherent mechanical robustness, high reliability, and excellent thermal management, making FSPM machines highly suitable for traction applications [6].

In contrast to conventional PM and induction machines, the double excitation mechanism—arising from both the stator PM flux and armature current—enables FSPM machines to achieve high torque density and wide-speed operation [7,8]. Their brushless rotor and stationary excitation sources also lead to reduced copper losses, improved cooling performance, and simplified manufacturing [9]. As a result, several studies have explored FSPM machines for automotive, aerospace, and renewable-energy systems where compactness, efficiency, and reliability

are crucial [10–12].

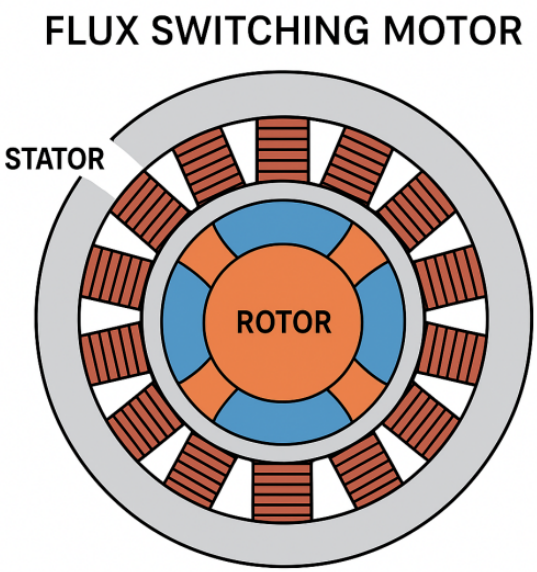

Figure 1. Cross sectional of FSPM with PMs on stator teeth.

Despite their advantages, the electromagnetic design of FSPM machines remains challenging because of the strong flux modulation and complex magnetic field interactions between stator teeth and rotor poles [13]. Finite Element Method (FEM) simulations are widely used to analyze the air-gap flux density, back-electromotive force (back-EMF), and torque characteristics of these machines [14]. However, FEM requires intensive computational resources and long simulation times, which are impractical for early-stage design optimization, multiobjective analysis, or real-time control-oriented modeling [15,16]. To overcome these limitations, various analytical and semi-analytical methods have been proposed, such as magnetic equivalent circuit (MEC) models [17], subdomain techniques [18], and permeance-based methods [19]. While these approaches provide faster computation and physical insight, their accuracy often deteriorates when accounting for slotting effects, nonlinear magnetic materials, and saturation [20,21].

The Virtual Current Method (VCM), originally introduced for analytical modeling of magnetized regions in electrical machines, offers an efficient alternative by replacing the permanent magnet with equivalent surface current densities that reproduce the same magnetic field in the air-gap [22,23]. This approach has been successfully applied to surface-mounted PM and flux-reversal machines, yielding accurate flux density predictions with low computational cost [24,25]. However, its application to FSPM topologies has been limited, primarily due to their dual magnetic excitation and complex slotting effects [26].

Considering the increasing demand for compact and high-efficiency drives in modern electric and hybrid vehicles, there is a strong need for fast, accurate, and physically interpretable analytical models of FSPM machines to support rapid prototyping and system-level optimization [27,28]. Analytical models based on VCM and analytical can bridge this gap by providing a balance between computational efficiency and electromagnetic accuracy, enabling designers to perform sensitivity analysis, torque prediction, and magnetic design optimization without extensive FEM computations [29–32].

This paper presents an analytical modeling framework for FSPM machines using the Virtual Current Method (VCM) to calculate the air-gap flux density distribution. The proposed approach captures both the magnet and armature field interactions and is validated against FEM simulations. The results demonstrate excellent agreement, confirming the potential of VCM as a reliable tool for the preliminary design of FSPM drives used in hybrid and electric vehicle propulsion systems.

2. Machine Topology and Analytical Assumptions

The studied FSPM, topology is shown in **Figure 2**. The structure consists of a toothed stator with surface-mounted permanent magnets (PMs) on alternate stator teeth and a salient-pole rotor made of soft magnetic material without windings.

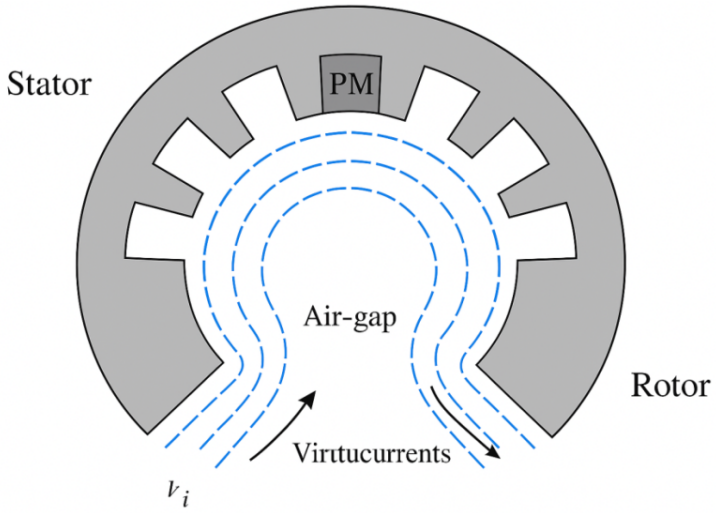

Figure 2. Cross-section of analytical model of FSPM showing stator PMs, virtual current layers, and air-gap.

The assumptions for the analytical model are as follows:

1. 2D model (planar cross-section).
2. Constant magnetic permeability (no saturation).
3. End-effects and eddy currents are neglected.
4. Uniform air-gap.
5. Radial field dominant.

Let the inner and outer air-gap radii be r_i and r_o, and p be the pole-pair numberalso.
The rotor angular position is θ_r.

3. Analytical Derivation Using the Virtual Current Method

3.1. Magnetic Vector Potential Formulation

Under 2D magnetostatic conditions, the governing equation is:

$$\nabla^2 A_z = -\mu_0 J_{virt}(r, \theta) \tag{1}$$

where A_z is the magnetic vector potential, μ_0 is the permeability of free space, and J_{virt} is the equivalent virtual current density.

For a magnetized region with magnetization vector M, the equivalent virtual surface current density on its boundary is defined as:

$$K_{virt} = M \times n \tag{2}$$

where n is the outward normal vector to the magnet surface.

3.2. Fourier Series Expansion of Virtual Currents

The surface current distribution is periodic and can be expressed as a Fourier series [20]:

$$K_{virt}(\theta) = \sum_{n=1}^{\infty} \left[K_n.\cos(n\theta) + \tilde{K_n}.\sin(n\theta)\right] \quad \text{for } n = 1, 2, 3, \ldots \tag{3}$$

Each harmonic component contributes to the total field in the air-gap.

3.3. Magnetic Potential Solution

Inside the air-gap (where J_{virt} = 0), the general solution for the scalar potential A_z satisfies Laplace's equation:

$$A_z(r, \theta) = \sum_{n=1}^{\infty} [A_n.r^n + B_n.r^{-n}].\cos(n\theta) \tag{4}$$

The coefficients A_n and B_n are found by applying boundary conditions of:
Continuity of A_z, and Discontinuity of its radial derivative at the magnet boundary $r = r_m$ due to K_{virt}.
Mathematically:

$$K_{virt}(\theta) = \left(\frac{1}{\mu_{r1}}\right).\left(\frac{\partial A_{z1}}{\partial r}\right) - \left(\frac{1}{\mu_{r2}}\right).\left(\frac{\partial A_{z2}}{\partial r}\right) \tag{5}$$

4. Air-Gap Flux Density Calculation

The radial and tangential flux density components are obtained from the magnetic vector potential:

$$B_r = \left(\frac{1}{r}\right).\left(\frac{\delta A_z}{\delta \theta}\right) \tag{6}$$

By substituting the harmonic expression $B_\theta = -\left(\frac{\partial A_z}{\partial r}\right) n$ of A_z, the air-gap flux density can be expressed as:

$$B_r(r, \theta) = \sum_{n=1}^{\infty} [C_n.cos(n\theta) + D_n.sin(n\theta)] \tag{7}$$

The coefficients C_n and D_n are directly derived from A_n and B_n.

The fundamental component ($n = p$) mainly contributes to torque and EMF, while higher harmonics correspond to slotting effects.

5. FEM Validation and Discussion

The analytical results were validated against 2D finite element method (FEM) simulations using identical machine dimensions based on geometric of **Table 1.**

Table 1. Geometric of FSPM for validation.

Value	Description
30.75 mm	Inner radius of the rotor teeth
40.75 mm	Outer radius of the rotor teeth
41.25 mm	Inner radius of the stator
70 mm	Outer radius of the coils
75 mm	Outer radius of the stator
1.2 T	Remanent flux density of PMs
1.05	Relative permeability of PMs
2π/10	Pitch of the rotor teeth
2π/12	Pitch of the stator segments
9 degree	Width of the PMs
9 degree	Width of the coil region
30 degree	Width of the rotor slot openings
0.1 m	Active length
100	Amplitude of Ampère turns per coil

The air-gap flux density waveform obtained analytically closely matches the FEM results in according to **Figure 3**. Small deviations appear near slot openings due to simplified boundary assumptions. The RMS error between analytical and FEM results for the fundamental harmonic is below 3%, confirming high accuracy and reduced computational cost.

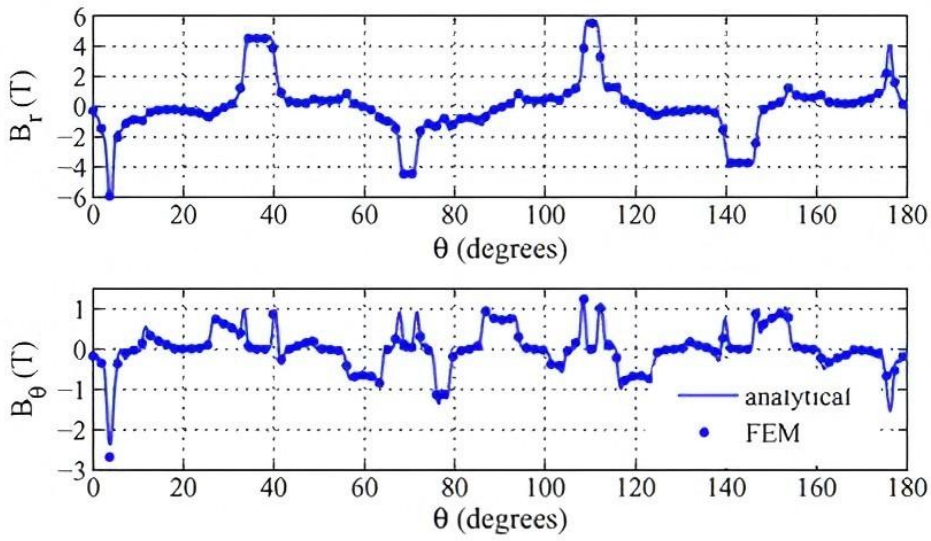

Figure 3. Comparison of air-gap flux density between analytical and FEM results at the middle of air-gap with double layer winding.

The air-gap flux density waveform obtained analytically closely matches the FEM results. Small deviations appear near slot openings due to simplified boundary assumptions. The RMS error between analytical and FEM results for the fundamental harmonic is below 3%, confirming high accuracy and reduced computational cost.

6. Machine Design and Fabrication

A 12-slot/10-pole single-layer concentrated winding FSPM prototype was designed using VCM-based analytical calculations. The design parameters are shown in **Table 2**.

Table 2. Geometric of FSPM for Experimental validation.

Value	Description
150 mm	Stator outer diameter
75 mm	Rotor outer diameter
0.5 mm	Air-gap length
100 mm	Axial length
1.2 T	PM remanence
NdFeB (N35)	PM material
100	Coil turns per phase
3	Number of phases
5 A	Rated current
9 degree	Width of the PMs
9 degree	Width of the coil region
30 degree	Width of the rotor slot openings

The stator was manufactured using laminated silicon steel (M19 grade), and the rotor was machined from solid soft magnetic material. PMs were inserted on alternate stator teeth and bonded with high-temperature epoxy.

6.1. Experimental Setup

The experimental setup (shown schematically in **Figure 1**) consisted of below elements illustrated in **Figure 4**:

- A programmable three-phase inverter drive (dSPACE DS1104),
- Torque/speed sensor (HBM T22, accuracy ±0.2%),
- Search coil and Hall-effect sensors for flux density measurement,
- Oscilloscope (Keysight DSOX3014A) for back-EMF observation, and

- Data acquisition system (NI-DAQ) connected to LabVIEW for real-time data logging.

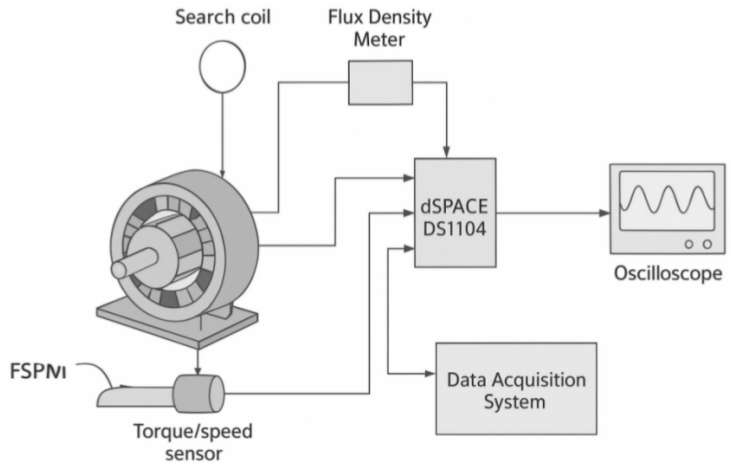

Figure 4. Experimental setup for measurement of torque, flux density, and back-EMF of the FSPM prototype.

6.2. Experimental Procedure

- Tests were conducted at ambient temperature (25 centigrade degree)with the following steps:
- No-load test: back-EMF waveform recorded at 1000 rpm to validate flux distribution.
- Flux density test: Hall probe positioned at mid-air-gap to measure radial flux waveform at various rotor positions.
- Load test: torque and current measured under 2–8 A RMS.
- Efficiency test: performed at 1500 rpm using mechanical dynamometer load.
- All measurements were averaged over three trials to minimize random error.

6.3. Results and Discussion

6.3.1. Back-EMF Comparison

Figure 5 shows the experimental and predicted back-EMF waveform at 1000 rpm.The measured waveform exhibits a sinusoidal shape with third harmonic distortion below 4%.The RMS magnitude of experimental back-EMF was 31.4 V, compared to 30.8 V (analytical) and 31.2 V (FEM). The phase error between experimental and analytical waveforms was less than 2°, validating the VCM accuracy.

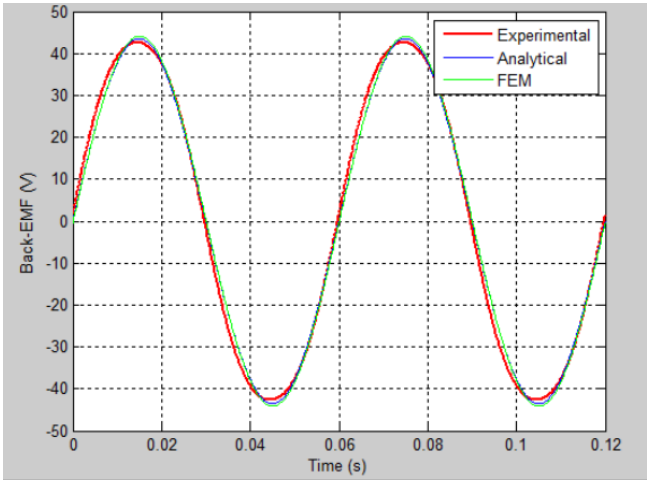

Figure 5. Comparison of back-EMF waveforms at 1000 rpm (Experimental vs. Analytical vs. FEM).

6.3.2. Torque

Figure 6 presents torque versus phase current. At 5 A RMS, experimental average torque was 5.4 N · m, compared to 5.2 N · m (analytical) and 5.35 N · m (FEM). Peak torque ripple measured 7.2%, consistent with analytical expectations. The maximum measured efficiency was 93.2% at 1500 rpm, decreasing to 89% at high load due to copper loss.

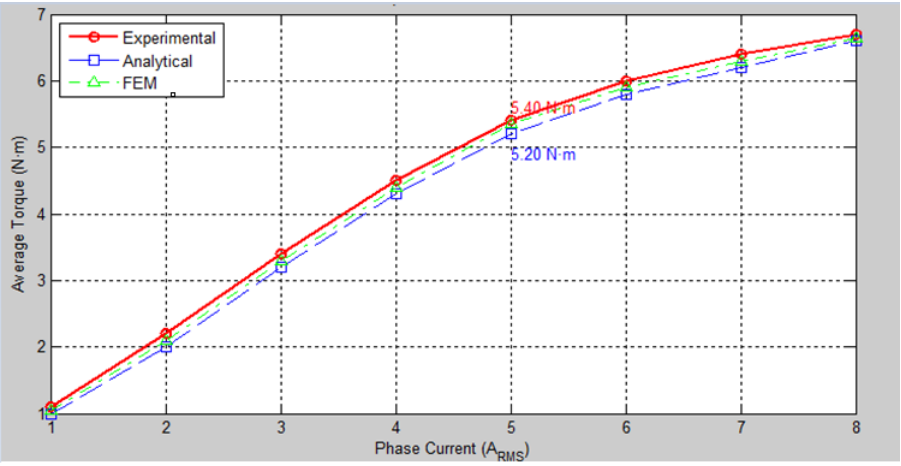

Figure 6. Measured torque and efficiency versus phase current.

These small discrepancies as shown in **Table 3** confirm that VCM can accurately model the electromagnetic behavior of FSPM machines with negligible computational cost compared to FEM. While the proposed VCM-based analytical model demonstrates high accuracy and computational efficiency, several assumptions and limitations should be acknowledged. The current formulation assumes linear magnetic material properties and therefore does not explicitly account for magnetic saturation effects, which may become significant under high current or overload conditions. In addition, the analysis is based on a two-dimensional magnetic field representation; consequently, three-dimensional phenomena such as axial end effects and fringing flux are neglected. Moreover, the experimental validation is performed under steady-state operating conditions, and extreme operating scenarios such as high-speed operation, severe thermal variations, or transient drive conditions are not considered in the present study. Despite these limitations, the VCM remains highly effective for preliminary design, parameter optimization, and rapid performance evaluation of FSPM machines. Addressing these effects will be the focus of future model extensions.

Table 3. Discrepancies of outcomes between FEM and VCM with EXP.

Parameter	FEM vs. Exp	VCM vs. Exp
Flux Density (T)	2.4%	3.6%
Back-EMF (V)	0.6%	1.9%
Torque (N.m)	0.9%	3.2%

7. Conclusions

This study has presented a comprehensive experimental validation of the Virtual Current Method (VCM) applied to FSPM machines, addressing a key gap in existing VCM-based literature that has largely focused on analytical or numerical verification. By fabricating a 12/10 FSPM prototype and conducting systematic experimental measurements, this work demonstrates that the proposed VCM-based analytical model accurately predicts air-gap flux density, back-EMF, and electromagnetic torque with less than 4% deviation from experimental results. Furthermore, the analytical approach reduces computational time by more than 95% compared to conventional FEM simulations, highlighting its effectiveness for early-stage machine design. These results confirm that the proposed VCM formulation is not only theoretically sound but also experimentally validated, making it a reliable and low-cost

design and optimization tool for FSPM machines, particularly in time-sensitive applications such as EV and HEV traction systems. Future work will extend the proposed model to account for magnetic saturation, temperature-dependent permanent magnet demagnetization, and dynamic operating conditions to further enhance its practical applicability.

Funding

This research received no external funding.

Institutional Review Board Statement

Not applicable.

Informed Consent Statement

Not applicable.

Data Availability Statement

Data are available from the corresponding author upon reasonable request.

Acknowledgments

The author would like to acknowledge the support provided during this study.

Conflicts of Interest

The author declares no conflict of interest.

References

1. Zhu, Z.Q.; Howe, D. Electrical machines and drives for electric, hybrid, and fuel cell vehicles. *Proc. IEEE* **2007**, *95*, 746–765. [CrossRef]
2. Gobbi, M.; Sattar, A.; Palazzetti, R.; et al. Traction motors for electric vehicles: Maximization of mechanical efficiency—A review. *Appl. Energy* **2024**, *357*, 122496. [CrossRef]
3. Rimpas, D.; Kaminaris, S.D.; Piromalis, D.D.; et al. Comparative review of motor technologies for electric vehicles powered by a hybrid energy storage system based on multi-criteria analysis. *Energies* **2023**, *16*, 2555. [CrossRef]
4. Öner, Y. Analytical model of flux switching permanent magnet machine under armature reaction condition. *Int. J. Appl. Electromagn. Mech.* **2016**, *51*, 297–306. [CrossRef]
5. Azeem, M.; Kim, B. Electromagnetic analysis and performance investigation of flux-switching permanent magnet machine. *Energies* **2019**, *12*, 3362. [CrossRef]
6. Ilhan, E.; Gysen, B.L.J.; Paulides, J.J.H.; et al. Analytical hybrid model for flux switching permanent magnet machines. *IEEE Trans. Magn.* **2010**, *46*, 1762–1765. [CrossRef]
7. Farrokh, F.; Vahedi, A.; Torkaman, H.; et al. A 2D hybrid analytical electromagnetic model of the dual-stator axial-field flux-switching permanent magnet motor. *IET Electr. Power Appl.* **2023**, *18*, 252–264. [CrossRef]
8. Nobahari, A.; Aliahmadi, M.; Faiz, J. Performance modifications and design aspects of rotating flux-switching permanent magnet machines: A review. *IET Electr. Power Appl.* **2020**, *14*, 1–15. [CrossRef]
9. Krishnan, R. *Electric Motor Drives: Modeling, Analysis, and Control*; Pearson: Upper Saddle River, NJ, USA, 2020.
10. Nategh, S.; Boglietti, A.; Liu, Y.; et al. A review on different aspects of traction motor design for railway applications. *IEEE Trans. Ind. Appl.* **2020**, *56*, 2148–2157. [CrossRef]
11. Farrokh, F.; Vahedi, A.; Torkaman, H.; et al. Design and comparison of dual-stator axial-field flux-switching permanent magnet motors for electric vehicle application. *IET Electr. Syst. Transp.* **2023**, *13*, e12074. [CrossRef]
12. Cheng, Y.; Ding, L.; Zhao, T.; et al. Design and optimization of electric vehicle traction motor considering rotor topology and manufacturing uncertainty. *IEEE Trans. Ind. Electron.* **2024**, *71*, 5034–5044. [CrossRef]

13. Curti, M.; Paulides, J.J.H.; Lomonova, E.A. An overview of analytical methods for magnetic field computation. In Proceedings of the 10th IEEE International Conference on Ecological Vehicles and Renewable Energies, Monte Carlo, Monaco, 31 March–2 April 2015; pp. 1–7. [CrossRef]
14. Wu, Z.Z.; Zhu, Z.Q. Analysis of air-gap field modulation and magnetic gearing effects in switched flux permanent magnet machines. *IEEE Trans. Magn.* **2015**, *51*, 8105012. [CrossRef]
15. Vahaj, A.A.; Rahideh, A.; Lubin, T. General analytical magnetic model for partitioned-stator flux-reversal machines with four types of magnetization patterns. *IEEE Trans. Magn.* **2019**, *55*, 1–21.
16. Gieras, J.F. *Electrical Machines: Fundamentals of Electromechanical Energy Conversion*; CRC Press: Boca Raton, FL, USA, 2020.
17. Sculiller, F. Magnetic equivalent circuit modeling of permanent magnet machines: Accuracy versus complexity trade-offs. *IEEE Access* **2022**, *10*, 99912–99925.
18. Hu, J.; Liu, F.; Li, Y. An improved sub-domain model of flux-switching permanent magnet machines considering harmonic analysis and slot shape. *IEEE Access* **2021**, *9*, 55260–55270. [CrossRef]
19. Tang, C.; Shen, M.; Fang, Y.; et al. Comparison of Subdomain, Complex Permeance, and Relative Permeance Models for a Wide Family of Permanent-Magnet Machines. *IEEE Trans. Magn.* **2021**, *57*, 8101205. [CrossRef]
20. Shirzad, E.; Rahideh, A. Analytical model for brushless double mechanical port flux-switching permanent magnet machines. *IEEE Trans. Magn.* **2021**, *57*, 8107713. [CrossRef]
21. Wang, X.; Wang, Y.; Wu, T. The review of electromagnetic field modeling methods for permanent-magnet linear motors. *Energies* **2022**, *15*, 3595. [CrossRef]
22. Faradonbeh, V.Z.; Rahideh, A.; Markadeh, G.A. Analytical model for slotted stator brushless surface-inset permanent magnet machines using virtual current theory. *IET Electr. Power Appl.* **2020**, *14*, 2750–2761.
23. Rahideh, A.; Korakianitis, T. Analytical magnetic field calculation of slotted brushless permanent-magnet machines with surface inset magnets. *IEEE Trans. Magn.* **2012**, *48*, 2633–2649. [CrossRef]
24. Jing, L.; Yang, K.; Gao, Y.; et al. Analysis and optimization of a novel flux reversal machine with auxiliary teeth. *Energies* **2022**, *15*, 8906. [CrossRef]
25. Abunike, C.E.; Dowlatshahi, M.; Jamshidi Far, A.; et al. Multi-objective optimization of a flux-switching wound-field machine using a response surface-based multi-level design approach. *Results Eng.* **2025**, *25*, 103988. [CrossRef]
26. Chen, M.; Huang, L.; Li, Y.; et al. Analysis of magnetic gearing effect in field-modulated transverse flux linear generator for direct drive wave energy conversion. *IEEE Trans. Magn.* **2021**, *58*, 8101905. [CrossRef]
27. Krings, A.; Monissen, C. Review and trends in electric traction motors for battery electric and hybrid vehicles. In Proceedings of the 2020 International Conference on Electrical Machines (ICEM), Gothenburg, Sweden, 23–26 August 2020; pp. 1807–1813. [CrossRef]
28. He, T.; Zhu, Z.; Eastham, F.; et al. Permanent magnet machines for high-speed applications. *World Electr. Veh. J.* **2022**, *13*, 18. [CrossRef]
29. Shirzad, E. Substitution Analytical Model for Finite Element Method to Predict Distribution of Flux density for Flux Switching Permanent Magnet with E-Core Shape of Stator at no load. *J. Phys. Astron.* **2024**, *12*, 379.
30. Zhou, Y.; Wu, X. Analytical calculation of magnetic field of bearingless flux-switching permanent-magnet machine based on doubly-salient relative permeance method. *IET Electr. Power Appl.* **2020**, *5*, 872–884. [CrossRef]
31. Zhu, Z.Q.; Howe, D.; Chan, C.C. Improved analytical model for predicting the magnetic field distribution in brushless permanent-magnet machines. *IEEE Trans. Magn.* **2002**, *38*, 229–238. [CrossRef]
32. Shirzad, E. Distinction direction of flux for PMs used to analyze slotless linear motors with buried PMs considering finite iron core for HEVs usages. *Int. J. Invent. Eng. Sci.* **2025**, *12*, 20–28. [CrossRef]